

# Thermoelastic Martensitic Transformation and Shape Memory Effect in $\text{Sr}_2(\text{Si}, \text{Ge})\text{O}_4$

Koichiro FUKUDA, Tetsuya FUKUDA, Akio SUZUKI and Akira YAMAGUCHI

Department of Materials Science and Engineering, Nagoya Institute of Technology, Gokiso-cho, Showa-ku, Nagoya-shi 466-8555

## $\text{Sr}_2(\text{Si}, \text{Ge})\text{O}_4$ の熱弾性型マルテンサイト変態と形状記憶効果

福田功一郎・福田哲也・鈴木章雄・山口明良

名古屋工業大学材料工学科, 466-8555 名古屋市昭和区御器所町

Crystals of  $\text{Sr}_2(\text{Si}_{1-x}\text{Ge}_x)\text{O}_4$  with  $0 \leq x \leq 1$  were prepared and examined by powder XRD, optical microscopy, and AFM. The crystals with  $0.3 \leq x \leq 0.6$  were composed of both the  $\alpha'$  (orthorhombic)- and twinned  $\beta$  (monoclinic)-phases. On the basis of the lattice correspondence between the two phases and their cell parameters, the phenomenological crystallographic theory has been applied to determine the habit planes and shape deformations upon  $\alpha'$ -to- $\beta$  martensitic transformation. The habit planes, which define the coherent interphase boundaries between  $\alpha'$  and  $\beta$ , were nearly parallel to either (100) or (001). Because the transformation was accompanied by a small volumetric shrinkage of  $\sim 0.3\%$ , the parent  $\alpha'$ -phase would elastically accommodate the strains upon the polysynthetic twin formation of the  $\beta$ -phase. At 293 K, the crystals with  $x = 0.6$  were composed of  $\sim 92.5$  mass%  $\alpha'$  and  $\sim 7.5$  mass%  $\beta$ . During further cooling in liquid nitrogen, the  $\alpha'$ -to- $\beta$  transformation proceeded which increases the phase composition of  $\beta$  up to  $\sim 56.3\%$ . The transformation is accompanied by the formation of plate-like surface reliefs. The surface relief angles have been determined from both observations ( $7.4 \pm 0.2^\circ$ ) and calculations based on a phenomenological analysis ( $7.55^\circ$ ). The fair agreement of these values indicates that the transformation is martensitic and mainly governed by a shear mechanism. The shape memory effect has been demonstrated by the reproducibility of the surface reliefs. The coherency at the interface boundaries between the  $\alpha'$ - and  $\beta$ -phases as well as the effective strain accommodation substantially account for the thermoelasticity of the solid solutions.

[Received August 20, 2001; Accepted September 26, 2001]

**Key-words:** Thermoelastic martensitic transformation, Surface relief angles, Shape memory effects, Ceramics

### 1. Introduction

Displacive phase transformations between the orthorhombic ( $\alpha'$ )- and monoclinic ( $\beta$ )-phases of  $\text{Sr}_2(\text{Si}, \text{Ge})\text{O}_4$  are interesting, because the solid solutions may be regarded as representatives in the broad class of  $\beta$ - $\text{K}_2\text{SO}_4$ -related compounds. Pieper et al. have investigated the solid solubility and polymorphism in the system  $\text{Sr}_2\text{SiO}_4$ - $\text{Sr}_2\text{GeO}_4$ .<sup>1)</sup> For the crystals with  $0 \leq \text{Ge}/(\text{Ge} + \text{Si}) \leq 0.3$  (in molar ratio), the transformation temperatures between  $\alpha'$  and  $\beta$  were determined, which steadily decreased with increasing Ge content. By extrapolation of the transition curve, an unusually low temperature of 228 K was predicted for the  $\alpha'$ -to- $\beta$  transformation of pure  $\text{Sr}_2\text{GeO}_4$ .<sup>1)</sup> However, no satisfactory explanation has so far been offered for the transformation mechanism.

The  $\alpha'$ -to- $\beta$  phase transition of pure  $\text{Sr}_2\text{SiO}_4$  involves a change in space group from  $Pmnb$  to  $P2_1/n$ .<sup>2),3)</sup> in which the point group reduces from  $mmm$  (order 8) to  $2/m$  (order 4). Thus, the symmetry change during the transition is accompanied by the reduction of the point group order by a factor of 2, which gives rise to two twin orientations. The twin variants should be related to each other by the lost mirror planes of the parent  $\alpha'$ -phase. Accordingly, the twinning has been pseudo-merohedral,<sup>4)</sup> in which the twins are related by the (100) $_{\beta}$  pseudo-symmetry plane. Another possible twinning, related by the (001) $_{\beta}$  pseudo-symmetry plane, has never been reported.<sup>5)</sup>

The crystal structures and polymorphic sequence of  $\text{Sr}_2(\text{Si}, \text{Ge})\text{O}_4$  are analogous to those of  $\text{Ca}_2\text{SiO}_4$  solid solutions.<sup>1),6)</sup> In the latter, the phase change from  $\alpha'_L$  (orthorhombic) to  $\beta$  (monoclinic) has been reported to be a thermoelastic martensitic transformation.<sup>7-11)</sup> The relief effect, which is characteristic of martensitic transforma-

tions, has been confirmed on the pre-polished crystal surface.<sup>7),12)</sup> In situ observation has been done, under a high-temperature microscope, to demonstrate the reproducibility of the surface reliefs.<sup>7)</sup> The phenomenological crystallographic theory, as used in martensitic transformations, has been successful in the prediction of the shape deformations and habit-plane orientations.<sup>10),11)</sup> The prediction indicated the complete degree of lattice matching (complete coherency) at the interphase boundaries.

The application of stress at any temperature in the transformation range usually increases the amount of displacive transformations.<sup>13)</sup> With  $\text{Ca}_2\text{SiO}_4$  solid solutions, the transformation has been induced by internal thermal stress upon quenching.<sup>14)</sup> Because the transformation is athermal, the fraction transformed remains unchanged when the temperature is kept constant. Accordingly, the phase constitution at a certain temperature ( $T$ ) during cooling has been principally determined to be  $\beta$  ( $T < M_f$ ),  $\alpha'_L$  and  $\beta$  ( $M_f \leq T \leq M_s$ ) and  $\alpha'_L$  ( $M_s < T$ ), where  $M_s$  and  $M_f$  are the starting and finishing temperatures of the martensitic transformation, respectively.<sup>8)</sup>

In the present study, we have applied the phenomenological theory to the  $\alpha'$ -to- $\beta$  transition in  $\text{Sr}_2(\text{Si}, \text{Ge})\text{O}_4$ . The discussion of the thermoelasticity of the transformation is based not only on the calculation results but also on the observation results as demonstrating the shape memory effect.

### 2. Experimental procedure

#### 2.1 Materials

Crystals of  $\text{Sr}_2(\text{Si}_{1-x}\text{Ge}_x)\text{O}_4$  with  $0 \leq x \leq 1$  were prepared from appropriate amounts of reagent-grade chemicals  $\text{CaCO}_3$ ,  $\text{SiO}_2$  and  $\text{GeO}_2$ . The mixtures were, after calcination at 1473 K for 20 min, pressed into pellets, heated at 1773 K

(the stable temperature region of the  $\alpha'$ -phase) for 5 h, then quenched in air (293 K). The series of these samples as obtained were termed S-A. Some of the sintered pellets of S-A were pulverized and soaked in liquid nitrogen for 10 min (Sample S-B).

## 2.2 Characterization

The profile intensity data were collected on an X-ray powder diffractometer (XRD; Model RAD-B, Rigaku, Tokyo, Japan) using Ni-filtered  $\text{Cu K}\alpha$  radiation (40 kV, 20 mA) and a step-scan technique (step width =  $0.02^\circ$  and fixed time = 5 s) in the  $2\theta$  range from  $18$  to  $60^\circ$ . Si powder was used as the internal standard (Sample/Si = 8 by weight). The weight fractions of the  $\alpha'$ - and  $\beta$ -phases (respectively  $W_{\alpha'}$  and  $W_{\beta}$ ) as well as the unit-cell dimensions of the individual phases were refined by a Rietveld method on a computer program RIETAN.<sup>15</sup> The atomic positions of both phases<sup>2,16</sup> were fixed throughout the refinement process. The relative amount of the  $\alpha'$ -phase with respect to the  $\beta$ -phase,  $W_{\beta}/(W_{\alpha'} + W_{\beta})$ , was defined as the fraction transformed of the  $\alpha'$ -to- $\beta$  transition.

One of the sintered pellets of the crystals with  $x = 0.6$  was polished with diamond paste to form a flat surface, then soaked in liquid nitrogen for 10 min. The resulting reliefs on the pre-polished surface were observed using a differential interference microscope. The fine structure of the relief in a  $20 \mu\text{m} \times 20 \mu\text{m}$  area was examined using an atomic force microscope (AFM; Model SPA-300, Seiko Instruments, Inc., Chiba). The same pellet was then heated at 353 K for 10 min in an oven. The change in surface deformation was examined at ambient temperature using the optical microscope. The cooling and heating cycle was repeated five times to confirm the reproducibility of the shape deformation.

## 3. Results and discussion

### 3.1 Change in fraction transformed and cell dimensions with Ge/(Ge+Si) ratio

The crystals with  $0.3 \leq x \leq 0.7$  were composed of both the  $\alpha'$ - and  $\beta$ -phases (Fig. 1). The fraction transformed of S-B was necessarily higher than that of S-A. This indicates that the  $\alpha'$ -to- $\beta$  phase transition proceeds upon cooling below ambient temperature, which is consistent with the martensitic nature in which thermal activation is unnecessary for the transformation. With increasing  $x$ -value, the fraction transformed of both samples steadily decreased. The crystals with  $0 \leq x \leq 0.2$  were exclusively composed of the

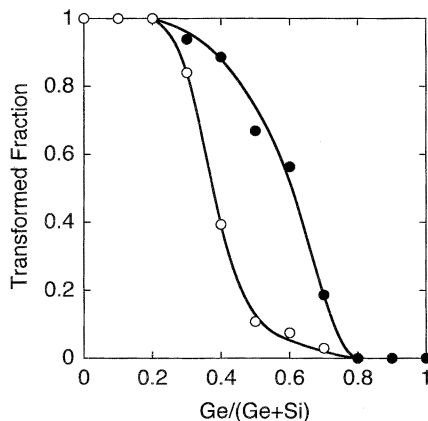


Fig. 1. Fraction transformed of  $\alpha' \rightarrow \beta$  with Ge/(Ge+Si) ratio. The fraction is defined by  $W_{\beta}/(W_{\alpha'} + W_{\beta})$ , where  $W_{\alpha'}$  and  $W_{\beta}$  are the weight fractions of the  $\alpha'$ - and  $\beta$ -phases, respectively. (○) Sample S-A and (●) S-B.

$\beta$ -phase, and those with  $0.8 \leq x \leq 1$  were made up of the  $\alpha'$ -phase. The phase constitution at ambient temperature (293 K) indicates that the transformation temperatures  $M_s$  and  $M_f$  satisfy the following relationship:  $293 \text{ K} < M_f$  ( $0 \leq x \leq 0.2$ ),  $M_f < 293 \text{ K} < M_s$  ( $0.3 \leq x \leq 0.7$ ) and  $M_s < 293 \text{ K}$  ( $0.8 \leq x \leq 1$ ). This implies that  $M_s$  and  $M_f$  steadily decrease with increasing  $x$ -value, in accord with a previous study.<sup>1)</sup>

All of the cell dimensions ( $a$ ,  $b$ , and  $c$ ) for both phases steadily increased with increasing  $x$ -value (Fig. 2). The differences in cell dimensions between S-A and S-B cannot be regarded as significant. For the crystals with  $0.3 \leq x \leq 0.6$ , individual cell dimensions of the coexisting two phases were successfully refined, and they are, for example with  $x = 0.6$ , given in Table 1. Upon  $\alpha'$ -to- $\beta$  transition, there was a slight reduction in cell volume of less than 0.3% (Fig. 2 (e)).

### 3.2 Principal distortions upon $\alpha'$ -to- $\beta$ transition

The phenomenological crystallographic theory has been applied to the crystals with  $0.3 \leq x \leq 0.6$ . The magnitudes and directions of the principal distortions ( $\lambda_i$ ) upon  $\alpha'$ -to- $\beta$  phase transition are respectively given by the eigenvalues and eigenvectors of the following equation:<sup>17)</sup>

$$|(\text{OC}'\text{M})(\text{M}^*\text{GM})(\text{MCO}) - \lambda_i^2(\text{O}^*\text{GO})| = 0 \quad (1)$$

The matrix (MCO) represents the lattice correspondence between the orthorhombic  $\alpha'$ -phase (O) and the monoclinic  $\beta$ -phase (M). Because there are two orientational variants (denoted by I and II) related by the polysynthetic twinning for the  $\beta$ -phase, we consider two matrices for the lattice correspondence:

$$(\text{MCO})_{\text{I}} = \begin{bmatrix} 1 & 0 & 0 \\ 0 & 1 & 0 \\ 0 & 0 & 1 \end{bmatrix}$$

$$(\text{MCO})_{\text{II}} = \begin{bmatrix} 1 & 0 & 0 \\ 0 & -1 & 0 \\ 0 & 0 & 1 \end{bmatrix}$$

The matrix (OC'M) is the transpose of (MCO). The metric (O\*GO) is for the  $\alpha'$ -phase and that of (M\*GM) is for the  $\beta$ -phase.<sup>9)</sup> In the orthonormal basis parallel to the principal axes, the lattice distortion matrix (B) takes the simple form of a diagonal matrix, consisting of the three eigenvalues ( $\lambda_1$ ,  $\lambda_2$  and  $\lambda_3$ ).

Equation (1) was solved to determine the magnitudes and directions of the principal distortions. For example, with the crystals of  $x = 0.6$ , they are given in Table 2. With increasing  $x$ -value, the magnitude of  $\lambda_1$  steadily increased and that of  $\lambda_3$  steadily decreased (Fig. 3). On the other hand, the  $\lambda_2$ -values ( $= b_{\beta}/b_{\alpha'}$ ) remained nearly unity, ranging from 1.001 ( $x = 0.3$ ) to 1.002 ( $x = 0.5$ ), where  $b_{\beta}$  and  $b_{\alpha'}$  are respectively the  $b$ -axis lengths of the  $\beta$ - and  $\alpha'$ -phases. This strongly suggests that, within the limits of measurement error, the simple relationship  $b_{\alpha'} = b_{\beta}$  holds for the coexisting  $\alpha'$ - and  $\beta$ -phases. The other distortions  $\lambda_1$  and  $\lambda_3$  are respectively larger and smaller than unity. Accordingly, on the assumption that the magnitudes of  $\lambda_2$  are invariably equal to unity, these principal distortions meet the general requirement for the occurrence of the undistorted planes.<sup>18)</sup> The subsequent rigid body rotation, represented by the matrix R, will ensure that these planes remain unrotated as well as undistorted. The resulting invariant planes define the habit planes, across which the  $\alpha'$ - and  $\beta$ -phases coherently fit.

### 3.3 Habit planes and twinning structures

Because the present shape deformation, represented by RB, is equivalent to the invariant plane deformation, we have

$$\text{RB} = \text{I} + m\text{dp}' \quad (2)$$

where I is the identify matrix,  $m$  is the magnitude of dis-

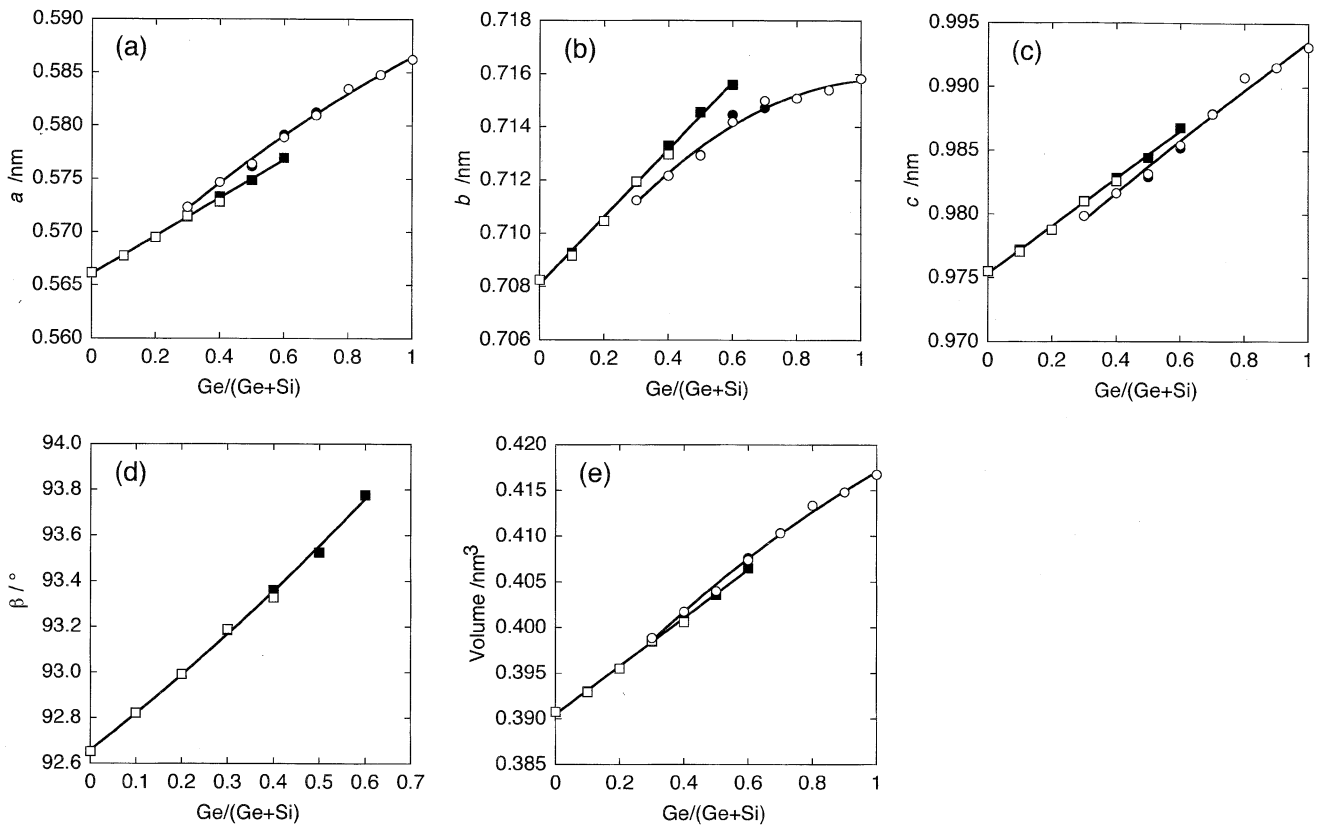


Fig. 2. Variation in cell dimensions with Ge/(Ge+Si) ratio.  $a$  (a),  $b$  (b),  $c$  (c),  $\beta$  (d) and volume (e). (○ and ●) Cell dimensions of the  $\alpha'$ -phase and (□ and ■) those of the  $\beta$ -phase. (○ and □) Sample S-A and (● and ■) S-B.

Table 1. Cell-Parameters of Coexisting  $\alpha'$ - and  $\beta$ -Phases in  $\text{Sr}_2(\text{Si}_{0.4}\text{Ge}_{0.6})\text{O}_4$

Phase	$a$ (nm)	$b$ (nm)	$c$ (nm)	$\beta$ (°)	Volume (nm <sup>3</sup> )
$\alpha'$	0.57913(6)	0.71447(7)	0.98515(9)	—	0.40763(7)
$\beta$	0.57696(5)	0.71560(8)	0.98675(9)	93.777(4)	0.40651(7)

Table 2. Principal Distortions ( $\lambda_i$ ) of  $\alpha'$ -to- $\beta$  Lattice Deformation in  $\text{Sr}_2(\text{Si}_{0.4}\text{Ge}_{0.6})\text{O}_4$

Variant	Principal distortion			Correspondence matrix
	$\lambda_1$	$\lambda_2$	$\lambda_3$	
I	$ \lambda_1  = 1.031$ $\lambda_1 = 0.678 \mathbf{i} - 0.735 \mathbf{k}$	$ \lambda_2  = 1.002 (\approx 1)$ $\lambda_2 = \mathbf{j}$	$ \lambda_3  = 0.965$ $\lambda_3 = 0.735 \mathbf{i} + 0.678 \mathbf{k}$	(MCO) <sub>I</sub>
II	$ \lambda_1  = 1.031$ $\lambda_1 = 0.678 \mathbf{i} + 0.735 \mathbf{k}$	$ \lambda_2  = 1.002 (\approx 1)$ $\lambda_2 = \mathbf{j}$	$ \lambda_3  = 0.965$ $\lambda_3 = 0.735 \mathbf{i} - 0.678 \mathbf{k}$	(MCO) <sub>II</sub>

$\mathbf{i}$ ,  $\mathbf{j}$  and  $\mathbf{k}$  are the unit vectors in the orthonormal basis defined by  $\mathbf{i} \parallel a_{\alpha'}$ ,  $\mathbf{j} \parallel b_{\alpha'}$  and  $\mathbf{k} \parallel c_{\alpha'}$ .

$\lambda_1$ ,  $\lambda_2$  and  $\lambda_3$  are the unit vectors along the principal axes.

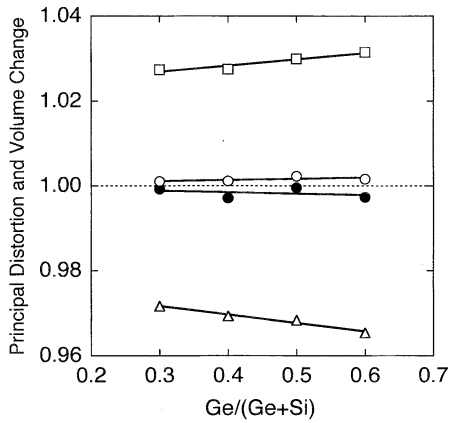


Fig. 3. Compositional dependence of principal distortions ( $\lambda_i$ ) and volume change ( $\lambda_1\lambda_2\lambda_3$ ) upon  $\alpha'$ -to- $\beta$  transition. The relationship  $\lambda_1 > 1$ ,  $\lambda_2 \approx 1$  and  $\lambda_3 < 1$  holds regardless of the  $\text{Ge}/(\text{Ge} + \text{Si})$  ratio. ( $\square$ )  $\lambda_1$ , ( $\circ$ )  $\lambda_2$ , ( $\triangle$ )  $\lambda_3$  and ( $\bullet$ )  $V_\beta/V_{\alpha'}$  ( $=\lambda_1\lambda_2\lambda_3$ ).

placement,  $\mathbf{d}$  is the unit vector parallel to the displacement and  $\mathbf{p}'$  is the unit row vector parallel to the habit plane normal.<sup>19</sup> Equation (2) was solved to determine the four types of shape deformations, termed A, B, C and D, in all. They are, for example with the crystals of  $x=0.6$ , given in Table 3. The deformations A and B produce respectively the twin variants I and II in Table 2. Both deformations yield the habit planes almost parallel to  $(100)_{\alpha',\beta}$ ; the intersection angles between the planes are  $\pm 1.4^\circ$  (Fig. 4(a)). The other habit planes formed by the deformations C and D are nearly parallel to  $(001)_{\alpha',\beta}$  with the intersection angles of  $\pm 3.3^\circ$  (Fig. 4(b)).

The individual shape change associated with each deformation determined above would create large stresses in both the parent and the product phases. In order to reduce the elastic stress, the product  $\beta$ -phase would form groups, each of which consists of the two variants.<sup>20</sup> The polysynthetic twinning on  $(100)_\beta$  can come about by having alternate regions in the parent  $\alpha'$  phase undergo the lattice deformations A and B. The resulting twin-related variants I and II require additional rigid body rotations around the  $b_{\alpha'}$ -axis at

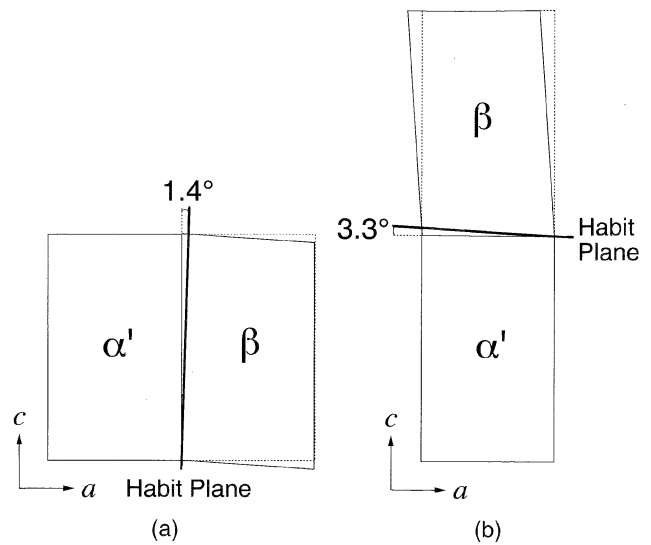


Fig. 4. Schematic of invariant plane deformations (a) A and (b) C in Table 3. The habit planes separating the  $\alpha'$ - and  $\beta$ -phases are almost parallel to  $(100)$  in (a) and  $(001)$  in (b). The interface boundaries between the two phases are completely coherent.

angles of  $+0.01^\circ$  and  $-0.01^\circ$ , respectively, to ensure that they coherently fit along the twinning plane, which is perpendicular to the  $a_{\alpha'}$ -axis. The highly magnified schematic picture of the  $(100)_\beta$  twin structure and the parent  $\alpha'$ -phase would appear as shown in Fig. 5(a). In a manner similar to that above, the polysynthetic twinning on  $(001)_\beta$  is formed by the alternate deformations C and D (Fig. 5(b)). In the nucleation of the  $\beta$ -phase in the parent  $\alpha$ -phase, the formation of such twinning can require different energies. Thus, these energy differences can favor the formation of one twin orientation over the other.

### 3.4 Surface reliefs

The presence or absence of observable surface relief is entirely dependent on the direction of the shape deformation relative to the surface. Because the deformation direction of the  $(100)$  twinning is along  $\langle 001 \rangle$  and that of the  $(001)$

Table 3. Direction and Magnitude of Shape Deformation in  $\text{Sr}_2(\text{Si}_{0.4}\text{Ge}_{0.6})\text{O}_4$

Type	Habit plane normal ( $\mathbf{p}'$ )	Displacement		Shape deformation matrix ( $\mathbf{RB}$ )	Correspondence matrix
		Direction ( $\mathbf{d}$ )	Magnitude ( $m$ )		
A	$\begin{bmatrix} 0.9997 \\ 0 \\ -0.0247 \end{bmatrix} \sim \begin{bmatrix} 1 \\ 0 \\ 0 \end{bmatrix}$	$[-0.0897, 0, -0.9960]$	0.0661	$\begin{bmatrix} 0.9941 & 0 & -0.0001 \\ 0 & 1 & 0 \\ -0.0658 & 0 & 1.0016 \end{bmatrix}$	$(\text{MCO})_{\text{I}}$
B	$\begin{bmatrix} 0.9997 \\ 0 \\ 0.0247 \end{bmatrix} \sim \begin{bmatrix} 1 \\ 0 \\ 0 \end{bmatrix}$	$[-0.0897, 0, 0.9960]$	0.0661	$\begin{bmatrix} 0.9941 & 0 & -0.0001 \\ 0 & 1 & 0 \\ 0.0658 & 0 & 1.0016 \end{bmatrix}$	$(\text{MCO})_{\text{II}}$
C	$\begin{bmatrix} 0.0567 \\ 0 \\ 0.9984 \end{bmatrix} \sim \begin{bmatrix} 0 \\ 0 \\ 1 \end{bmatrix}$	$[-1.0000, 0, 0.0083]$	0.0661	$\begin{bmatrix} 0.9963 & 0 & -0.0659 \\ 0 & 1 & 0 \\ 0.0000 & 0 & 1.0016 \end{bmatrix}$	$(\text{MCO})_{\text{I}}$
D	$\begin{bmatrix} -0.0567 \\ 0 \\ 0.9984 \end{bmatrix} \sim \begin{bmatrix} 0 \\ 0 \\ 1 \end{bmatrix}$	$[1.0000, 0, 0.0083]$	0.0661	$\begin{bmatrix} 0.9963 & 0 & 0.0659 \\ 0 & 1 & 0 \\ -0.0000 & 0 & 1.0016 \end{bmatrix}$	$(\text{MCO})_{\text{II}}$

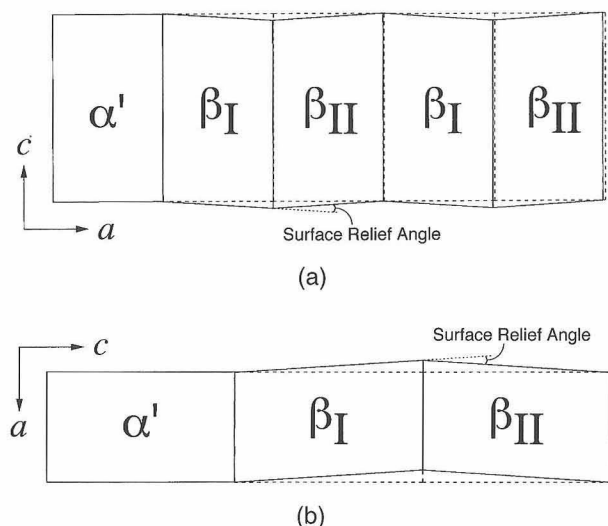


Fig. 5. Schematic of twinning structures of the  $\beta$ -phase. The alternate shape deformations of A and B in Table 3 result in the formation of (100) polysynthetic twinning in (a) and those of C and D produce the (001) twinning in (b). The surface relief angle is defined by the supplementary angle between the two flat surfaces of the twin-related variants.

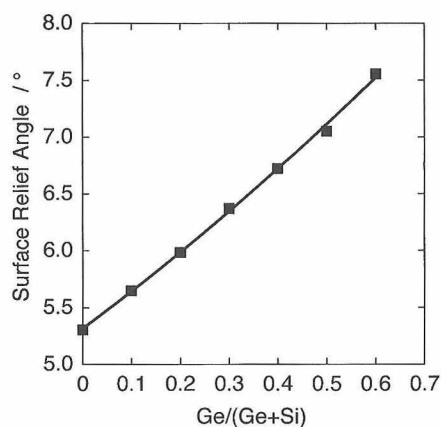


Fig. 6. The surface relief angles as a function of  $\text{Ge}/(\text{Ge} + \text{Si})$  ratio. The angles are simply determined by  $2\beta - 180^\circ$ , where  $\beta$  is the inter-axial angle  $\alpha$  of the  $\beta$ -phase.

twinning is along  $\langle 100 \rangle$ , the reliefs are formed on the crystal surface parallel to (001) for the former and (100) for the latter. Both types of twinning provide the same magnitude of surface relief angle, which is simply determined by  $2\beta - 180^\circ$ , where  $\beta$  is the angle  $\beta$  for the twinned  $\beta$ -phase (Figs. 5(a) and 5(b)). The surface relief angles as a function of  $x$ -value are given in Fig. 6. For the crystals with  $x = 0.6$ , the reliefs show the maximum angle of  $\sim 7.5^\circ$ .

When the crystals with  $x = 0.6$  were cooled to near the liquid-nitrogen temperature, the phase composition of  $\beta$  increased from  $\sim 7.5\%$  to  $\sim 56.3\%$  (Fig. 1), and the plate-like reliefs appeared on the polished surface (Fig. 7(a)). The relief profile, corresponding to the line in the figure, shows that each relief is  $\sim 2 \mu\text{m}$  in width and  $\sim 50 \text{ nm}$  in height (Fig. 7(b)). Each shape of the profiles is almost bilaterally symmetrical. This implies that the twin variant interfaces, which exist at the peak of the profiles, would be nearly perpendicular to the polished surface, and each side

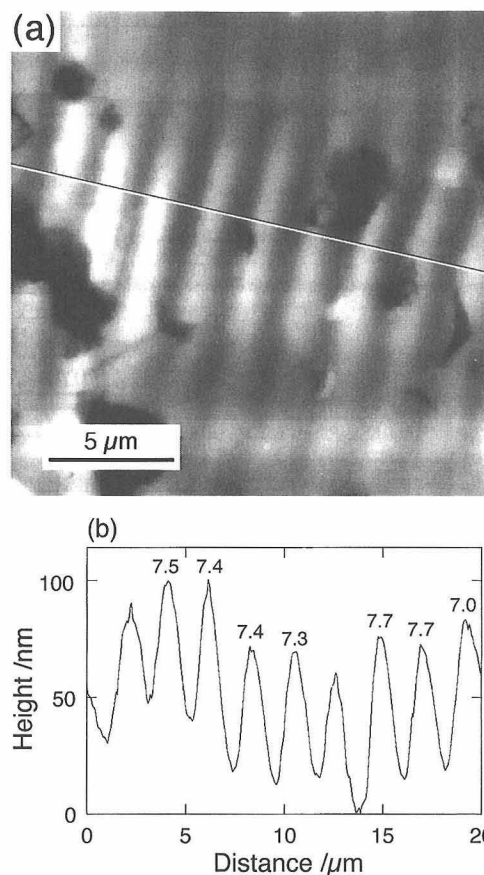


Fig. 7. (a) An AFM image of the surface reliefs for the  $\text{Sr}_2(\text{Si}_{0.4}\text{Ge}_{0.6})\text{O}_4$  crystal. (b) A cross section perpendicular to the twin variant interfaces along the line in (a). Numerals indicate the surface relief angles in degree.

of the peak would be entirely composed of the single orientational variant. The polished surface in Fig. 7(a) would therefore be almost parallel to either (001) or (100). The numerals above the individual relief profiles in Fig. 7(b) indicate the surface relief angles in degree. Their average is  $7.4^\circ$  with the standard deviation of  $0.2^\circ$ . This is in fair agreement with that determined from the calculation, indicating that the  $\alpha'$ -to- $\beta$  transformation is definitely martensitic and mainly governed by a shear mechanism.

### 3.5 Shape memory effect

The plate-like reliefs in Fig. 8(a) were formed during cooling in liquid nitrogen. After heating at  $\sim 353 \text{ K}$ , they completely disappeared (Fig. 8(b)); the original flat surface was eventually restored upon the reverse ( $\beta$ -to- $\alpha'$ ) transformation. During successive cooling in liquid nitrogen, exactly the same reliefs reappeared (Fig. 8(c)). The heating and cooling cycles were repeated five times to confirm the reproducibility of the reliefs. The behavior of this kind is termed shape memory effect,<sup>21)</sup> which is characteristic of thermoelastic martensitic transformations.

The phenomenological theory predicted that the transformation front of the parent  $\alpha'$ -phase and the twinned  $\beta$ -phase can be completely coherent. This coherency would be actually realized because the  $\alpha'$ -to- $\beta$  transformation was accompanied by a very small volume change. Thus, the strain accommodation would be elastically and almost completely achieved without dislocation generation at the interface boundaries. Such glissile boundaries<sup>13),21)</sup> can reversibly move forward and backward with a change in temperature.

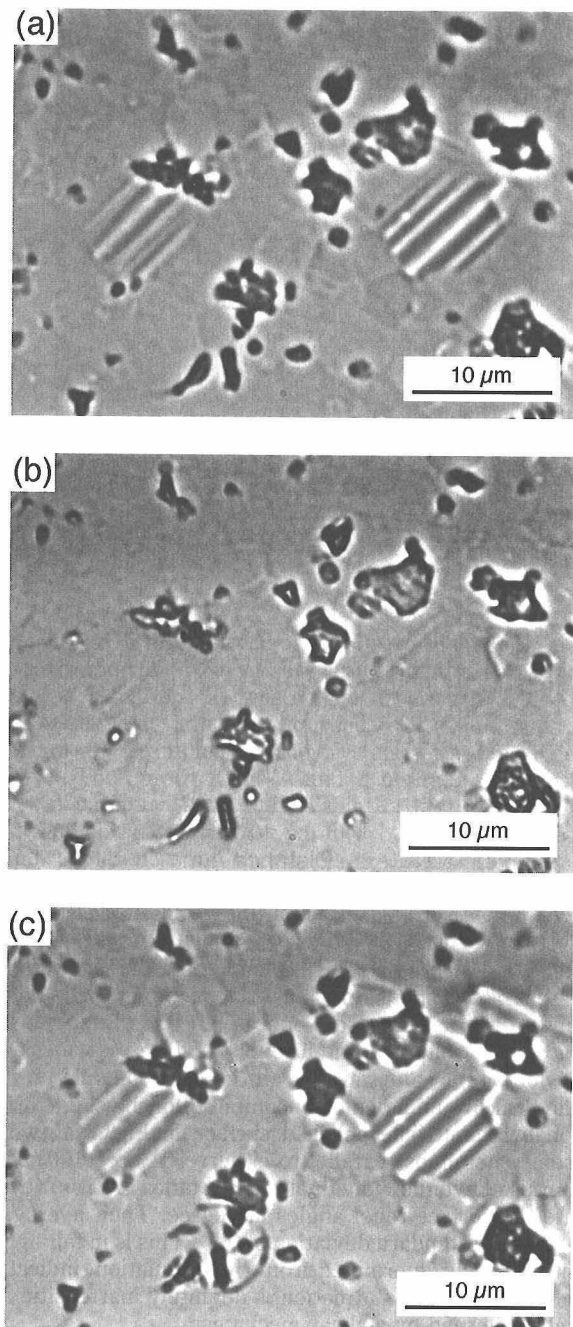


Fig. 8. A series of micrographs showing the shape memory effect of the  $\text{Sr}_2(\text{Si}_{0.4}\text{Ge}_{0.6})\text{O}_4$  crystals. (a) Two crystal grains show plate-like reliefs, which are formed in association with the  $\alpha'$ -to- $\beta$  transition upon cooling in liquid nitrogen. (b) The reliefs completely disappear during heating to  $\sim 353$  K. (c) The same reliefs appear again upon cooling in liquid nitrogen. Differential interference microscopy. All photographs were taken at 293 K.

The coherency at the interface boundaries as well as the effective strain accommodation would be essential to the thermoelasticity of  $\text{Sr}_2(\text{Si}, \text{Ge})\text{O}_4$ .

#### 4. Conclusions

(1) The phenomenological crystallographic theory of martensitic transformation was applied to the orthorhombic ( $\alpha'$ -phase)  $\rightarrow$  monoclinic ( $\beta$ -phase) phase transformation in  $\text{Sr}_2(\text{Si}_{1-x}\text{Ge}_x)\text{O}_4$ . The cell parameters of the coexisting phases with  $0.3 \leq x \leq 0.6$  satisfied  $b_{\alpha'} = b_{\beta}$ , which eventually

made one of the principal distortions equal to unity.

(2) The  $\alpha'$ -to- $\beta$  lattice deformation met the general requirement of the invariant plane deformation. This ensured the complete coherency with the lattices across the habit planes, which are almost in parallel with either (100) or (001).

(3) The transition was accompanied by the formation of plate-like surface reliefs. On the pre-polished surface parallel to either (001) or (100), the reliefs provided a surface relief angle of  $7.4 \pm 0.2^\circ$  for the  $\text{Sr}_2(\text{Si}_{0.4}\text{Ge}_{0.6})\text{O}_4$  crystal.

(4) The fair agreement between the surface relief angles determined from the observation and the calculation ( $7.55^\circ$ ) indicates that the  $\alpha'$ -to- $\beta$  transformation is definitely martensitic and mainly governed by a shear mechanism.

(5) The  $\alpha'$ -to- $\beta$  lattice change was accompanied by a small volumetric shrinkage of 0.3%. Thus, the parent  $\alpha'$ -phase would elastically accommodate the strains upon the polysynthetic twin formation of the  $\beta$ -phase.

(6) Both the coherency with the lattices at the transformation front and the effective strain accommodation probably cause the thermoelasticity (shape memory effect) of the solid solutions.

#### References

- Pieper, G., Eysel, W. and Hahn, Th., *J. Am. Ceram. Soc.*, **55**, 619–22 (1972).
- Catti, M., Gazzoni, G. and Ivaldi, G., *Acta Cryst. C*, **39**, 29–34 (1983).
- Catti, M., Gazzoni, G., Ivaldi, G. and Zanini, G., *Acta Cryst. B*, **39**, 674–79 (1983).
- Nord, G. L., Jr., "Imaging Transformation-Induced Microstructures, Minerals and Reactions at the Atomic Scale: Transmission Electron Microscopy," Ed. by Buseck, P. R., Mineralogical Society of America, Washington, D. C., U.S.A. (1992) pp. 455–508.
- Catti, M. and Gazzoni, G., *Acta Cryst. B*, **39**, 679–84 (1983).
- Stenberg, L. and Hyde, B. G., *Acta Cryst. B*, **42**, 417–22 (1986).
- Fukuda, K., Maki, I. and Ito, S., *J. Am. Ceram. Soc.*, **79**, 2925–28 (1996).
- Fukuda, K., Maki, I. and Ito, S., *J. Am. Ceram. Soc.*, **79**, 2969–70 (1996).
- Fukuda, K., Ito, S. and Taguchi, H., *Cem. Concr. Res.*, **28**, 1141–45 (1998).
- Fukuda, K., *J. Mater. Res.*, **14**, 460–64 (1999).
- Fukuda, K., *J. Ceram. Soc. Japan*, **108**, 701–04 (2000).
- Fukuda, K., Taguchi, H., Nomura, Y. and Ota, T., *J. Am. Ceram. Soc.*, **83**, 2097–99 (2000).
- Christian, J. W., "The Theory of Transformations in Metals and Alloys," 2nd ed., Pergamon Press, Oxford, U. K. (1975).
- Fukuda, K., Iizuka, E., Taguchi, H. and Ito, S., *J. Am. Ceram. Soc.*, **81**, 2729–31 (1998).
- Izumi, F., "Rietveld Analysis Programs RIETAN and PREMOS and Special Applications, The Rietveld Method," Ed. by Young, R. A., Oxford University Press, Oxford, U.K. (1993) pp. 236–53.
- Nishi, F. and Takéuchi, Y., *Zeit. Krist.*, **211**, 607–11 (1996).
- Mackenzie, J. K. and Bowles, J. S., *Acta Metal.*, **2**, 138–47 (1954).
- Bilby, E. C. and Christian, J. W., "The Mechanism of Phase Transformations in Metals: Martensitic Transformations," A Symposium Organized by the Institute of Metals and Held at the Royal Institution, London, on 9 Nov. 1955, London; No. 18 (1955) p. 121.
- Bowles, J. S. and Mackenzie, J. K., *Acta Metal.*, **2**, 129–37 (1954).
- Schroeder, T. A. and Wayman, C. M., *Acta Metal.*, **25**, 1375–91 (1977).
- Wayman, C. W., "Phase Transformations, Nondiffusive, Physical Metallurgy. Elsevier Science Publishers," Ed. by Cahn, R. W. and Haasen, P., Amsterdam, The Netherlands (1983) pp. 1031–74.